Composition and Physical Stability of the Colloidal Dispersion in Veiled Virgin Olive Oil

Carlotta Breschi, Giovanni Ferraro, Lorenzo Guerrini, Emiliano Fratini, Luca Calamai, Alessandro Parenti, Lorenzo Lunetti, and Bruno Zanoni*

Veiled virgin olive oil (VOO) samples of nine different olive cultivars are chosen to have a wide range of physicochemical and biological properties of colloidal dispersions. The contents of proteins and phospholipids range from 40 to 190 mg kg^{-1} and from 70 to 200 mg kg^{-1}, respectively. The effect of lab-scale centrifugation on cloudy appearance is studied measuring the decrease of turbidity grade values. The time to obtain unveiled oils (20 NTU) is modeled by a logistic equation, and a clear relationship between the initial water content and the above time is observed with a different trend between two groups of the VOO samples. Four VOO samples are selected to study the aggregation phenomena of microdroplets of water, pulp particles, and olive stone fragments via optical microscopy and dynamic light scattering during lab-scale gravity sedimentation. All VOOs are unstable with the cloudiness disappearing within the 230 days of investigation due to an overall diameter increase of cloudy components which is modeled by a power-law equation. The VOO samples, characterized by both small diameter values of dispersed components (150–250 nm) and high values of water content, show the fastest aggregation kinetics, but they have the longest time of cloudiness stability. *Practical Applications*: Water content and size distribution of VOO cloudy components can be key factors to control the colloidal stability. If removal of cloudy appearance is required, centrifugation can be applied to obtain a fast oil clarification which shows a power law relationship of water content with time. Instead, if physical stability of the colloidal dispersion is required, the aggregation phenomena should be slow down through VOO processing to obtain small diameters of the cloudy components. Tuning both the water content and dispersed phase diameter in the VOO can be the first step towards the control of phenomena related to the colloidal dispersion for every olive oil processing organization, above and beyond the simple removal of cloudy appearance by filtration.

1. Introduction

Veiled virgin olive oil (VOO) can be described as a water in oil (w/o) emulsion connected with a solid in oil dispersion where the cloudy appearance is caused by the scattering due to the intrinsic size of the two dispersed phases (i.e., water and solid).[1,2] The above system is thermodynamically unstable and, in turn, it causes chemical instability in the VOO. The cloudy appearance vanishes and a brown residue of solids and water settles at the bottom of tank or bottle during VOO storage time;[3] the water content increases the risk of VOO degradation phenomena causing both sensory defects due to microbial spoilage and hydrolytic phenomena of phenolic compounds.[4–6] Therefore, the companies that operate in olive oil processing and, particularly, distribute VOO need a careful control of the cloudy appearance.

Some studies on composition and physicochemical VOO properties are reported in the literature. Koidis et al.[7] and Breschi et al.[8] proposed a relevant characterization, based on the turbidity grade, the water and insoluble contents, the water activity, and the microbial contamination. There are few data on the minor compounds, which may have a role on VOO stability such as phospholipids and proteins. Phospholipids content was measured

C. Breschi, L. Calamai, A. Parenti, B. Zanoni
Department of Agriculture, Food, Environment and Forestry (DAGRI)
Università degli Studi di Firenze
P.le delle Cascine 18, Florence 50144, Italy
E-mail: bruno.zanoni@unifi.it

G. Ferraro, E. Fratini
Department of Chemistry "Ugo Schiff" and CSGI
Università degli Studi di Firenze
Via della Lastruccia 3, Sesto Fiorentino (FI) 50019, Italy

L. Guerrini
Department of Land, Environment, Agriculture and Forestry (TESAF)
Università di Padova
Via dell'Università 16, Legnaro (PD) 35020, Italy

L. Lunetti
Monini S.p.a.
Strada Statale Flaminia Km. 129, Spoleto (PG) 06049, Italy

Table 1. Physicochemical and biological properties of colloidal dispersion of the VOO samples; the small letters in the same row indicates statistically significant differences ($p < 0.05$) for the differentsamples; Ar = Arbequina, $C\#1$ = Coratina #1, $C\#2$ = Coratina #2, $C\#3$ = Coratina #3, $C+P$ = Coratina and Peranzana, K = Koroneiki, M = Manzanilla; N = Nocellara, Ogl = Ogliarola.

	Ar	$C\#1$	$C\#2$	$C\#3$	$C+P$	K	M	N	Ogl
Turbidity grade (NTU)	130 ± 12[ef]	1361 ± 50[b]	139 ± 10[e]	412 ± 27[c]	386 ± 39[c]	245 ± 31[d]	95 ± 15[f]	1773 ± 68[a]	112 ± 11[f]
Water content (% w/w)	0.20 ± 0.01[d]	0.42 ± 0.02[a]	0.24 ± 0.02[c]	0.33 ± 0.03[b]	0.26 ± 0.02[c]	0.18 ± 0.02[d]	0.11 ± 0.01[e]	0.36 ± 0.03[b]	0.22 ± 0.03[cd]
Insoluble content (% w/w)	0.04 ± 0.01[f]	0.19 ± 0.04[d]	0.17 ± 0.02[d]	0.18 ± 0.02[d]	0.10 ± 0.02[e]	0.32 ± 0.07[b]	0.25 ± 0.02[c]	0.31 ± 0.03[b]	0.54 ± 0.05[a]
Water activity (A_w)	0.68 ± 0.03[d]	0.80 ± 0.03[b]	0.64 ± 0.04[de]	0.78 ± 0.02[bc]	0.76 ± 0.01[c]	0.70 ± 0.02[d]	0.63 ± 0.02[e]	0.80 ± 0.02[b]	0.86 ± 0.03[a]
Microbial contamination (log CFU g^{-1})	4.3 ± 0.3[cd]	5.4 ± 0.1[a]	4.7 ± 0.1[c]	4.2 ± 0.1[d]	4.7 ± 0.1[c]	4.0 ± 0.2[d]	2.4 ± 0.3[e]	5.0 ± 0.1[b]	4.4 ± 0.2[cd]

according to their amphiphilic structure and ranged from 11 to 157 mg kg^{-1}; their content was higher in VOO than in filtered samples.[9,10] Protein content ranged from 0.05 to 2.40 mg kg^{-1} without a significant difference between filtered and unfiltered oils.[10,11] Lipid-soluble proteins and enzymes were identified as source of the protein content,[11,12] whereas a controversial role of proteins as emulsifiers of VOO was reported.[2,7,12]

Gravity sedimentation, centrifugation, and filtration are the common unit operations which are applied in oil processing companies (i.e., olive oil mills and blenders) to decrease the cloudy appearance after oil extraction. They are carried out alone or in combination to partially or totally remove the dispersed phases. The effect of the above operations on VOO was studied and some innovative plant solutions were proposed.[13–16] Many effects on oil quality were observed after filtration, in relation with its high efficacy to remove water and solids.[9] According to "Best Practice Guideline for the Storage" document (IOC/BPS/Doc. No 1/2018), filtration prevents microbial spoilage and hydrolytic phenomena, minimizing the formation of off-flavor and phenolic compounds hydrolysis during oil storage.[4,17–20] The role of filtration on oxidative phenomena is not still well understood. Since a decrease of phenolic compounds content may occur after filtration,[12,21,22] a reduction in oil oxidative stability is expected; instead, no negative oxidative effects during storage were shown by some authors[23,24] when comparing VOO with the correspondent filtered oil. An overall improvement of oil shelf-life was also related to removal of water and solids by means of gravity sedimentation and centrifugation, even though to a lesser extent in comparison with filtration.[13–15]

Recently, Cayuela-Sanchez and Caballero-Guerrero[2] suggested a more extended characterization of the cloudy appearance, which is also based on methods to estimate the so-called colloidal stability. Microdroplets of vegetation water, solid particles from fruit pulp, and stone fragments are the main components of the dispersed phase.[7] Reverse micelles and lamellar structures stabilize the w/o emulsion[12] whereas water droplets are usually adsorbed on the surface of the solid particles.[8] Literature studies suggested the role of both the amount and the structure of micelles on lipids oxidation.[25,26] The formation of micelles requires an appropriate amount of water and amphiphilic substances (i.e., phospholipids); an increase of lipid oxidation rate occurs when the size of the micelles increases due to an increase of water amount in the oil. Papadimitriou et al.[27] studied the structure and dynamics of the colloidal dispersions in VOO through different scattering techniques. They showed an effect of the oil extraction technique on the water droplets size; the three-phase decanter extraction formed larger and more polydispersed droplets than the two-phase decanter extraction. Gila et al.[13] observed a better performance of gravity sedimentation than centrifugation in reducing the content of moisture and solid organic impurities during VOO storage; the above results were explained by a highest emulsification degree in the centrifuged VOO as a result of the rotating movement imposed by the centrifuge.

For oil processing companies, the knowledge of colloidal structure and phenomena behind colloidal stability can allow either to improve the efficacy of the operations to reduce the cloudy appearance or to reach the physical stability of colloidal dispersion so as to prevent the loss of cloudy appearance. Since few data are reported in the literature on colloidal structure and stability in relation to oil processing and olive fruits cultivar, the aim of this study was to develop a structure–property relationship on the stability of the VOO colloidal dispersions thanks to an extended test campaigns carried out on several VOO samples processed from different olive oil fruits cultivars. In particular, the key points to investigate were:

1) the protein and phospholipids contents of VOO samples;
2) the kinetics of VOO turbidity grade decrease during lab-scale centrifugation;
3) the aggregation of VOO main components during lab-scale gravity sedimentation.

2. Results

The VOO samples of different olive cultivars and countries were chosen to have a wide range of physicochemical and biological properties of colloidal dispersions, as shown in **Table 1**. The cloudy appearance can be ranked in high (>500 NTU), medium (200–400 NTU), and low (90–140 NTU) turbidity grade values. The VOO samples can be also grouped according to the water/solid ratio: More water content than insoluble content values (Ar, $C\#1$, $C\#3$, $C+P$); more insoluble content than water content values (K, M, Ogl); similar water and insoluble content values ($C\#2$, N). All VOO samples had >4.0 (log CFU g^{-1}) microbial contamination except for the VOO sample with the lowest turbidity grade (M); the water activity values were ≥0.7 except for $C\#2$ and M samples.

Table 2. Amino acids, protein, and phospholipids content of the VOO samples; the small letters in the same row indicates statistically significant differences ($p < 0.05$) for the different samples; Ar = Arbequina, C#1 = Coratina #1, C#2 = Coratina #2, C#3 = Coratina #3, C+P = Coratina and Peranzana, K = Koroneiki; M = Manzanilla, N = Nocellara, Ogl = Ogliarola.

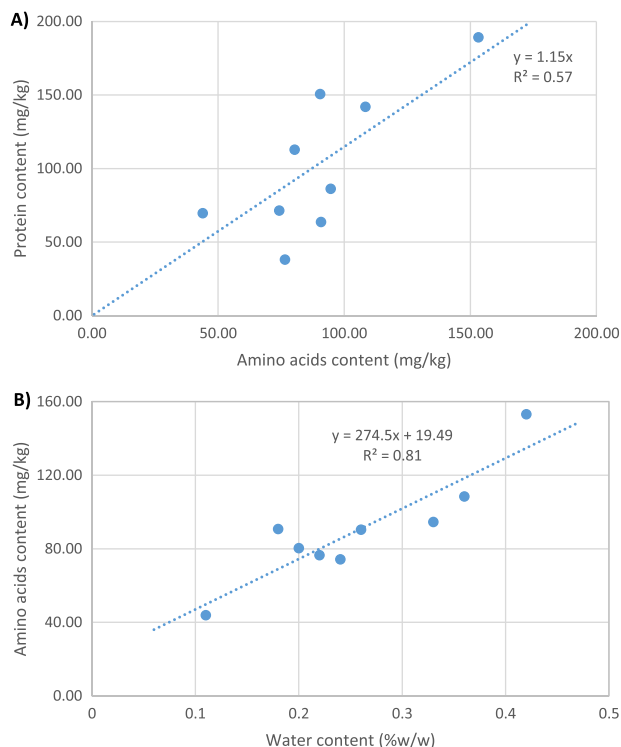|	Ar	C#1	C#2	C#3	C+P	K	M	N	Ogl
Total amino acids content (mg kg^{-1})	80 ± 6[d]	153 ± 11[a]	74 ± 5[d]	95 ± 3[c]	90 ± 6[cd]	91 ± 8[cd]	44 ± 2[e]	108 ± 9[b]	77 ± 4[d]
Protein content (mg kg^{-1})	113 ± 12[c]	189 ± 19[a]	72 ± 13[de]	86 ± 10[d]	151 ± 11[b]	64 ± 11[e]	70 ± 7[de]	142 ± 14[b]	38 ± 9[f]
Phospholipids content (mg kg^{-1})	196 ± 18[a]	145 ± 13[bc]	147 ± 15[bc]	148 ± 9[b]	135 ± 8[bc]	72 ± 12[d]	125 ± 13[c]	190 ± 13[a]	96 ± 12[d]

Figure 1. A) Relationship between total amino acids and proteins contents; B) relationship between total amino acids and water contents.

2.1. Protein and Phospholipids Contents

In the VOO samples, the contents of total amino acids and protein ranged from ≈45 to 150 mg kg^{-1} and from ≈40 to 190 mg kg^{-1}, respectively (**Table 2**). The micro-Lowry method proved to be effective in the measurement of the VOO protein content, showing results in agreement with those obtained from gas chromatography–mass spectrometry method: A linear relationship was observed between total amino acids and proteins contents (**Figure 1**A). The protein content of the VOO samples was one to two orders of magnitude higher than literature data,[10,11] but both Koidis and Boskou[10] and Hidalgo et al.[11] studied filtered and low veiled olive oil samples. Since a linear relationship was also observed between total amino acids and water contents (Figure 1B), the protein content could be largely due to enzymes according to the literature.[12,28] The phospholipids content ranged from ≈70 to 200 mg kg^{-1} (Table 2) in agreement with the literature data.[9,10]

2.2. Kinetics of VOO Turbidity Grade Decrease during Centrifugation

The effect of lab-scale centrifugation on cloudy appearance of the nine VOO samples was studied measuring the decrease of turbidity grade values (**Table 3**). The following logistic model was significantly able to describe kinetics of the VOO turbidity grade decrease (**Figure 2**)

$$\text{NTU} = \frac{a}{\left(1 + \left(\frac{t}{b}\right)^c\right)} \tag{1}$$

(where NTU is the turbidity grade, t is the centrifugation time, a, b, and c are proportionality constants which take into account the initial NTU value, the time corresponding to the inflection point of the curve, and the slope of the decay, respectively (Table 3).

The time to reach an asymptotic value of 20 NTU (corresponding to oil without visible cloudy appearance) was determined applying Equation (1) in order to study the adaptive behavior of the VOO samples being centrifuged (Table 3). A clear relationship between the initial water content (Table 1) and the above time ($t_{20\text{NTU}}$) was observed with a different trend between two groups of VOO samples (**Figure 3**). The first group, including Ar, C#1, C#2, C#3, N, and Ogl samples, showed a power-law relationship of water content with time (Figure 3A). The second group, including C+P, K, and M samples, showed a delayed trend and the centrifugation time to reach 20 NTU was longer than the above group for the same water content (Figure 3B).

2.3. Aggregation of VOO Main Components during Gravity Sedimentation

Two VOO samples from each of the two oil groups reported in Section 2.2 were selected to study the aggregation of VOO components during lab-scale gravity sedimentation, i.e., the C#1, N, K, and M samples. The above trial was carried out over a period of up to 230 days in order to have sufficient time to detect aggregation phenomena, without simulating effective preservation of the VOO samples in the company or on the market. Acquisition of microscope images and measurement of particle mean diameters were carried out on the VOO samples after sediment mixing; microscope images were also obtained on the VOO samples without sediment mixing.

Microdroplets of water, pulp particles, and olive stone fragments were the main components of cloudy appearance as shown by the optical micrographs acquired at 65 and 217 days of sedimentation, but size, shape, and aggregation behavior of the

Table 3. Turbidity grade decrease (NTU) of the VOO samples during lab-scale centrifugation; a, b, and c are proportionality constants of the logistic model (r^2 = determination coefficient) and t_{20NTU} is the time to reach 20 NTU; Ar = Arbequina, $C\#1$ = Coratina #1, $C\#2$ = Coratina #2, $C\#3$ = Coratina #3, $C+P$ = Coratina and Peranzana, K = Koroneiki, M = Manzanilla, N = Nocellara, Ogl = Ogliarola. min^c means that the constant b unit is min to the constant c value power.

|	0 min	1 min	3 min	5 min	7.5 min	15 min	30 min	a [NTU]	b [min^c]	c	r^2	t_{20NTU} [min]
Ar	130	42	30.3	27.5	23.2	18.9	16.6	130	0.13	0.36	0.99	14
$C\#1$	1361	395	324	247	237	164	123	1361	0.12	0.40	0.99	4914
$C\#2$	139	38	34.7	29.9	24.4	24	18.8	139	0.03	0.25	0.99	20
$C\#3$	294	141	92	67	56	36	19	294	0.92	0.71	0.99	37
$C+P$	386	223	168	139	120	90	50	385	1.85	0.60	0.9	237
K	245	174	134	111	96.6	59.6	36.1	244	3.78	0.77	0.99	88
M	95	35.7	34.3	27.4	25.7	22	18.9	95	0.20	0.27	0.99	26
N	1773	428	294	234	159	100	54.3	1773	0.15	0.58	0.99	352
Ogl	112	50.7	27.4	22.8	18.1	16.3	16	112	0.59	0.59	0.99	8
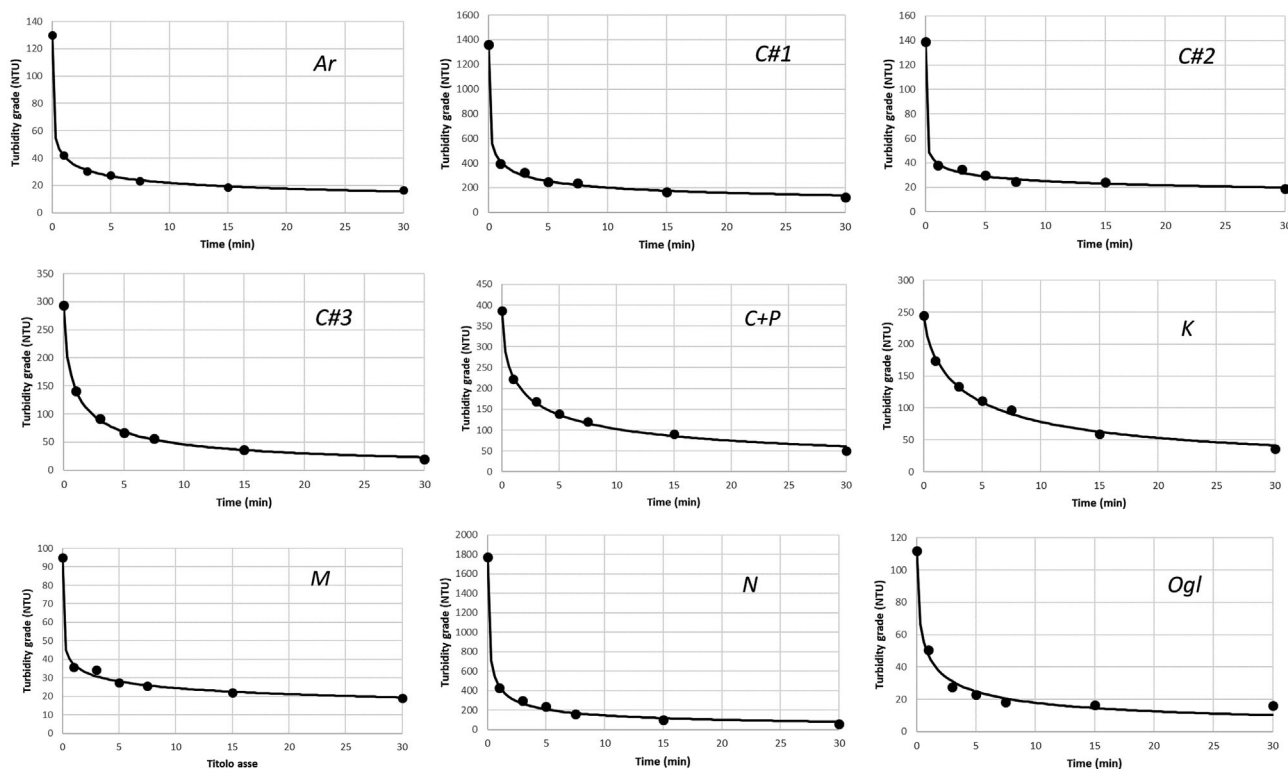
Figure 2. Application of the logistic model to describe kinetics of the VOO turbidity grade decrease during lab-scale centrifugation. Ar: Arbequina; $C\#1$: Coratina #1; $C\#2$: Coratina #2; $C\#3$: Coratina #3; $C+P$: Coratina and Peranzana; K: Koroneiki; M: Manzanilla; N: Nocellara; Ogl: Ogliarola.

main components were different in the VOO samples. In $C\#1$ mixed samples (**Figure 4A**), water component evolved from many droplets of small size to few and large droplets; pulp component evolved from several small particles to macroaggregates as well as olive stone fragments. In N mixed samples (Figure 4B), water droplets were not initially visible by microscope (despite the high value of water content in N samples), but it aggregated in many droplets of large size during sedimentation; pulp component evolved from several small particles to macroaggregates adsorbing water; irregular size and shape of stone fragments were

observed and stone component did not aggregate during sedimentation. In K mixed samples (Figure 4C), water component was not initially visible by microscope but water droplets during sedimentation were observed even if these samples had low water amounts (Table 1); pulp and stone components showed macroaggregates with a constant size during sedimentation. In M mixed samples (Figure 4D), water component evolved from few and small water droplets to no visible water droplets; pulp and stone components had a similar behavior, evolving from particles and fragments of small size to macroaggregates and, adsorbing water
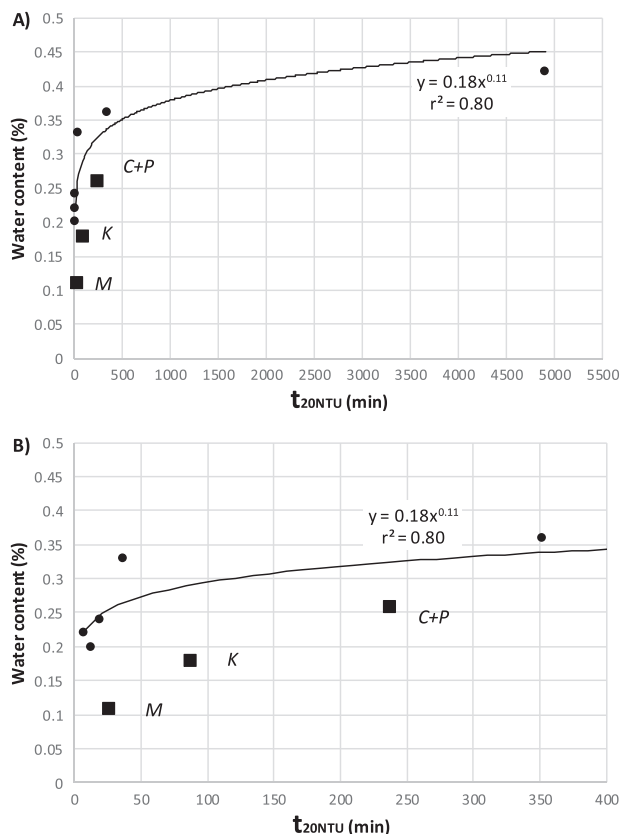
Figure 3. Relationship of VOO water content with time to reach the asymptotic value of 20 NTU during lab-scale centrifugation. Plot A) shows all experimental data, whereas plot B) chart focuses on the experimental data in the first section of centrifugation (■: C+P: Coratina and Peranzana; K: Koroneiki; M: Manzanilla; ● all the other VOO samples).

in the case of pulp particles. **Figure 5** shows the microscope images of VOO unmixed samples at 217 days of sedimentation. C#1, N, and M unmixed samples showed no cloudy appearance; no water droplets, macroaggregates of pulp, and stone components occurred (Figure 5A,B,D). Instead, K unmixed sample only showed a residual cloudy appearance, since water droplets and pulp aggregates were visible (Figure 5C).

The aggregation kinetics of the above four VOO samples were studied measuring the mean hydrodynamic diameter (dynamic light scattering (DLS)) of the main components generating the cloudy appearance during lab-sedimentation (**Table 4**). At time = 0, the C#1 and N samples had a dispersed phase with small diameter values, which could be related to the small size of water microdroplets and pulp particles as shown in microscope images (Figure 4A,B). Differently, the K and M samples had a dispersed phase with large diameter values, mainly due to the size of pulp particles and stone fragments (Figure 4C,D). An overall diameter increase of cloudy components occurred in the VOO samples during sedimentation and the following power law model was significantly able to describe the kinetics of the relative diameter increases (**Figure 6**).

$$D_{rel} = 1 + a \cdot t^b \qquad (2)$$

where D_{rel} is the ratio between the mean hydrodynamic diameter at the beginning and at different sedimentation times, t is the sedimentation time, a and b are proportionality constants (Table 4). Different kinetics occurred in the VOO samples. C#1 and N mixed samples had the fastest aggregation kinetics. Instead, K and M mixed samples had delayed kinetics characterized by an apparent lag-phase of aggregation phenomena. Relative diameters of cloudy components at fixed sedimentation times were also determined applying Equation (2) to have an aggregation capability index of the VOO samples; 120 and 240 days were chosen as short and long sedimentation time, respectively (Table 4). After 120 days, N mixed sample had the highest aggregation capability ($D_{rel} = 14.3$), followed by C#1 mixed sample ($D_{rel} = 3.6$); K and M mixed samples had the lowest aggregation capability ($D_{rel} = 1.4$ and 2.5, respectively), which was likely due to their high level of aggregation at time = 0 of sedimentation. However, for long sedimentation time (i.e., 240 days), the M mixed sample showed an aggregation capability higher than that of C#1 mixed sample ($D_{rel} = 7.3$ vs $D_{rel} = 4.6$, respectively), whereas N and K mixed samples continued to have the highest and the lowest aggregation capabilities, respectively.

3. Discussion

In the present study, the cloudy appearance was investigated in order to improve knowledge of structure and stability of VOO colloidal dispersions. The microscope images of VOO samples showed that the cloudy appearance was the result of the combined effect of the following main components, according to the literature data:[2,3,7,8] Water microdroplets in emulsion and solid particles in dispersion consisting of both pulp particles adsorbing water and inert stone fragments. The above colloidal system was physically unstable and sediments of water and solid particles resulted in the cloudy disappearance during 240 days of sedimentation (Figures 4 and 5). Measurable aggregation phenomena occurred during VOO sedimentation, which may suggest that the Ostwald ripening or coalescence had an essential role in the destabilization of the VOO colloidal dispersion. Both above processes result in the growth of large droplets at the "expense" of smaller ones, where in the first case the driving force depends on the fact that the solubility of the material within a spherical droplet in the surrounding continuous phase increases as the radius of the droplet decreases, whereas in the second case the droplets of the disperse phase collide and form larger droplets.[29] In the case of the solid fraction, the evolution follows simpler flocculation or aggregation phenomena. Consequently, the main components of VOO cloudy appearance evolved from small droplets/particles to large droplets/macroaggregates. As a consequence of this evolution, the dimension of the dispersed phase became too large to leave the components in the continuous phase, thus giving rise to the formation of sediments as a result of the density difference between the two phases (Table 4 and Figure 5). Then, a threshold limit of components mean diameter would be required to lose the VOO cloudy appearance.

The VOO samples showed aggregation phenomena which might be related to the combined effect of particle mean diameter, water, and insoluble contents. At the beginning of sedimentation tests, small diameter values of components
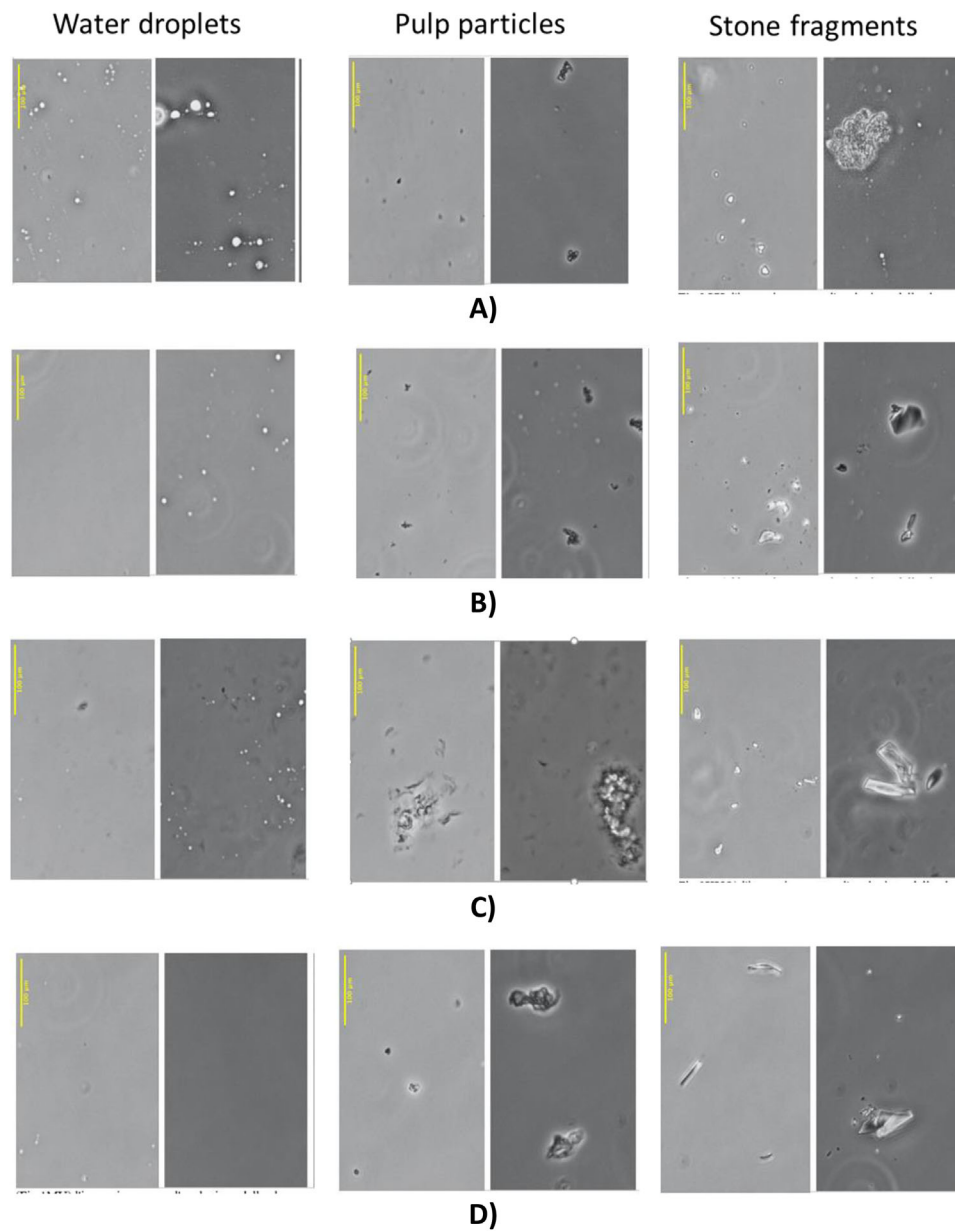
Figure 4. Optical micrographs after 65 and 217 days of lab-scale gravity sedimentation. A)–D) images show the behavior of Coratina, Nocellara, Koroneiki, and Manzanilla mixed samples, respectively.

(≈150–250 nm) characterized the VOO samples (*C#1* and *N* samples) at high values of water content and cloudy appearance (Tables 1 and 4); the relevant diameter values can be linked with the size of water droplets.[7] Instead, high diameter values of components (≈>1000 nm) featured the VOO samples (*K* and *M* samples) at low values of water content and cloudy appearance (Tables 1 and 4); the relevant diameter values can be mainly ascribed the size of solid particles.[7] During sedimentation tests, the aggregation kinetics was modeled using a power law to discriminate the behavior of the different VOO samples (Table 4 and Figure 6). The VOO samples, characterized by small diameter values of dispersed components, showed the fastest aggregation kinetics and high aggregation capabilities, but the suspended components remained dispersed for long time, since high values of diameters were reached only after several days. The longer times to reach the diameter threshold value would therefore guarantee higher stability of cloudy appearance of the above VOO samples. Instead, the VOO samples starting from high diameter values of components showed a delayed aggregation kinetics, since their components were already aggregated at the beginning of tests. However, different behaviors occurred between *K* and *M* samples; after the apparent lag-phase of aggregation, *M* samples maintained high aggregation capabilities, whereas *K* samples reached the lowest aggregation capability,
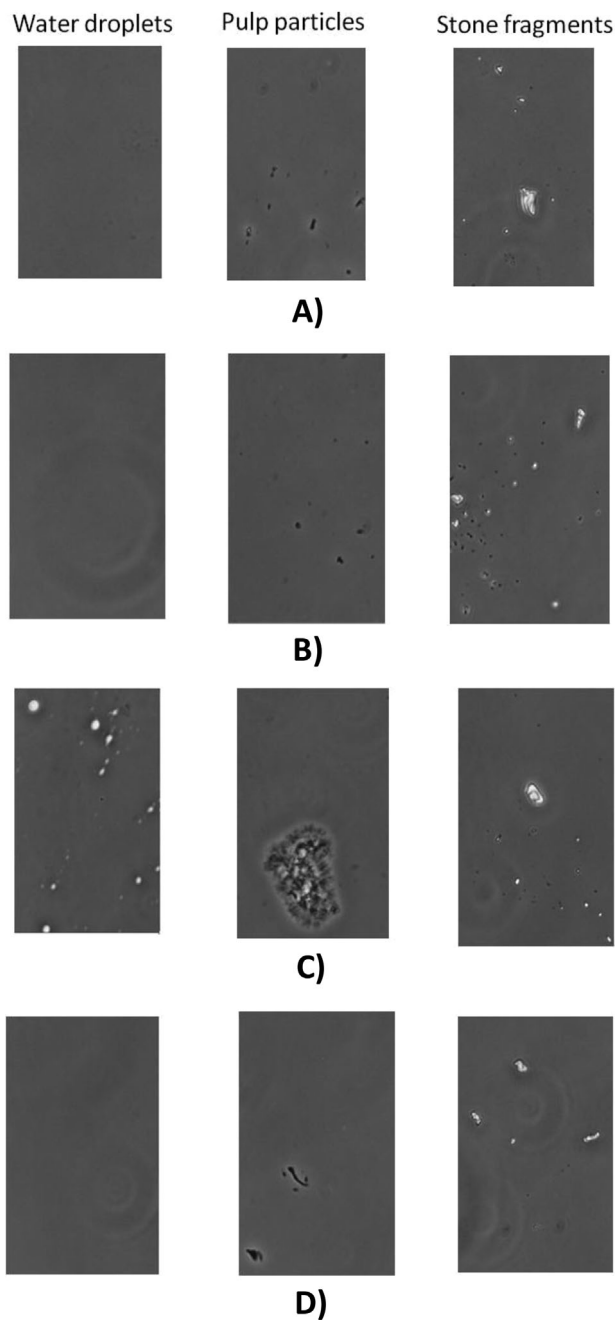
Figure 5. Optical micrographs after 217 days of lab-scale gravity sedimentation. A)–D) images show the behavior of Coratina, Nocellara, Koroneiki, and Manzanilla unmixed samples, respectively.

thus remaining cloudy after very long sedimentation time (Figure 5).

The above discussed structure and stability of colloidal dispersions were derived certainly from the processing history of the VOO samples, and a comparison between our experimental data and the VOO processing history may suggest further investigations as follows. It is interesting to study the role played by oil's extraction operations, such as that evidenced in the literature[27] relating to the two-phase decanter centrifuge causing small and

Table 4. Mean ($\bar{D}$) and relative (D_{rel}) diameters of cloudy components during lab-sedimentation; a and b are proportionality constants of the power model (r^2 = determination coefficient); C#1 = Coratina #1, K = Koroneiki, M = Manzanilla, N = Nocellara. n.d. not determined. 1/days^b means that the constant a unit is 1/days to constant b value power.

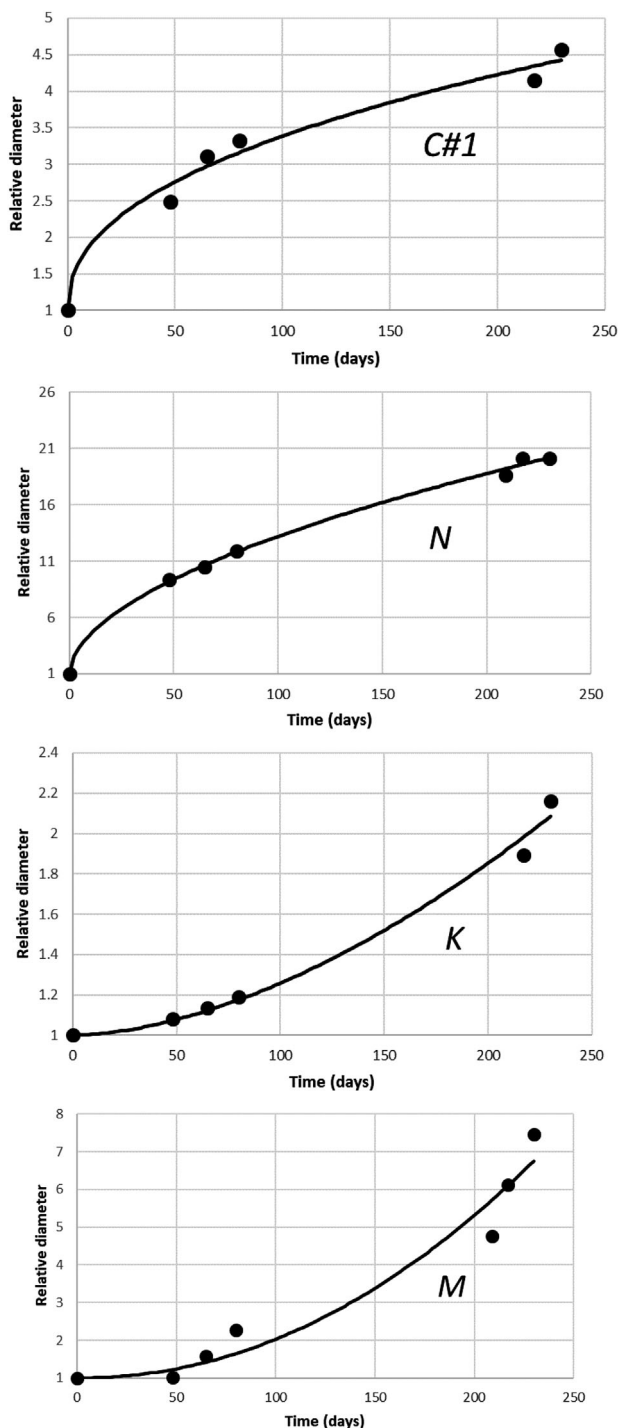|		0 days	48 days	65 days	80 days	209 days	217 days	230 days	a [1/days^b]	b	r^2	D_{rel} at 120 days	D_{rel} at 240 days
C#1	$\bar{D}$(nm)	241 ± 20	600 ± 250	750 ± 197	800 ± 250	n.d.	1000 ± 361	1100 ± 251	0.32	0.44	0.98	3.6	4.6
	D_{rel}	1.0	2.5	3.1	3.3	n.d.	4.1	4.6					
K	$\bar{D}$(nm)	925 ± 210	1000 ± 252	1050 ± 250	1100 ± 98	n.d.	1750 ± 64	2000 ± 478	9.4 10^{-5}	1.72	0.99	1.4	2.2
	D_{rel}	1.0	1.08	1.14	1.19	n.d.	1.89	2.16					
M	$\bar{D}$(nm)	4417 ± 1832	4500 ± 3008	7000 ± 2816	10000 ± 1974	21000 ± 4500	27000 ± 5000	33000 ± 5630	7.5 10^{-5}	2.07	0.95	2.5	7.3
	D_{rel}	1.0	1.0	1.6	2.3	4.8	6.1	7.5					
N	$\bar{D}$(nm)	134 ± 125	1250 ± 775	1400 ± 967	1600 ± 322	2500 ± 389	2700 ± 541	2700 ± 541	1.0	0.54	0.99	14.3	20.3
	D_{rel}	1.0	9.3	10.4	11.9	18.7	20.1	20.1					

Figure 6. Kinetics of relative diameter increase as a function of sedimentation time. *C#1*: Coratina #1; *K*: Koroneiki; *M*: Manzanilla; *N*: Nocellara.

poly-dispersed colloids. Similarly, it seems interesting to study the effect of the olive cultivar on colloidal dispersion in order to understand, for instance, the unusual behavior of the *Koroneiki* samples, which had long centrifugation times and a residual cloudy appearance even after several days of sedimentation.

4. Conclusions

This study evidenced that characterization of the structure and the physical stability of the VOO colloidal dispersions should be based on measurements of water content, insoluble content, and mean diameter of the main components of cloudy appearance (i.e., water microdroplets, solid particles, and inert stone fragments). The physical stability of VOO colloidal dispersion was proven to be achieved with the smallest diameter values of water droplets, whereas physical instability and complete removal of veiled components were caused by aggregation phenomena that increase diameter of the main components of the dispersed phase. Future studies should be carried out to analyze the relationship between structure of colloidal dispersion and chemical instability of VOO. If, in fact, the literature data clearly reported that the higher the water content, the greater the risk of decreased quality of virgin olive oil, this study suggest that also the diameter and the kinetics of aggregation phenomena should be considered for a potential effect on the rate of oil degradation phenomena during processing and shelf-life. In conclusion, tuning both the water content and dispersed phase diameter in the VOO could be the first step toward the control of phenomena related to the colloidal dispersion for every olive oil processing organization, above and beyond the simple removal of cloudy appearance by filtration. In olive oil mill, a specific design of oil extraction and preliminary VOO treatments may be applied to tailor the colloidal dispersion, whereas in olive oil blending companies the above characteristics may be applied both to qualify the purchased olive oil batches and to plan the subsequent processing activities.

5. Experimental Section

Materials: *VOO samples*: During the 2019–2020 crop season, freshly produced VOO batches of different olive cultivars were collected from the reception division of Monini S.p.A. (Spoleto, PG, Italy). The VOO batches were purchased from different suppliers or self-produced by Monini S.p.A during November 2019 as follows:

1) Arbequina batch (Ar) of 27 040 kg was extracted by two-phase decanter centrifuge in a Spanish oil mill from olive oil fruits harvested in Andalusia (Spain); the gravity sedimentation was applied on the above batch.
2) Coratina batch #1 (C#1) of 1730 kg was extracted by two-phase decanter centrifuge in an Italian oil mill from olive oil fruits harvested in Basilicata (Italy); the vertical centrifuge was applied on the above batch.
3) Coratina batch #2 (C#2) of 31 820 kg was extracted by two-phase decanter centrifuge in an Italian oil mill from olive oil fruits harvested in Apulia (Italy); the vertical centrifuge was applied on the above batch.
4) Coratina batch #3 (C#3) of 2760 kg was extracted by two-phase decanter centrifuge in an Italian oil mill from olive oil fruits harvested in Basilicata (Italy); the vertical centrifuge was applied on the above batch.
5) Coratina and Peranzana batch (C+P) of 5308 kg was extracted by two-phase decanter centrifuge in an Italian oil mill from blends of olive oil fruits harvested in Apulia (Italy); the vertical centrifuge was applied on the above batch.
6) Koroneiki batch (K) of 29 220 kg was a blend of VOOs extracted by three-phase decanter centrifuge in Greek oil mills from olive oil fruits harvested in Peloponnese (Greece); the vertical centrifuge was applied on the above batch.

**ADVANCED
SCIENCE NEWS**

www.advancedsciencenews.com

European Journal of
Lipid Science and Technology

www.ejlst.com

7) Manzanilla batch (M) of 26 920 kg was a blend of VOOs extracted by two-phase decanter centrifuge in Spanish oil mills from olive oil fruits harvested in Extremadura (Spain); the gravity sedimentation was only applied on the above batch.

8) Nocellara batch (N) of 1202 kg was extracted by two-phase decanter centrifuge in an Italian oil mill from olive oil fruits harvested in Basilicata (Italy); the vertical centrifuge was applied on the above batch.

9) Ogliarola batch (Ogl) of 26 872 kg was extracted by two-phase decanter centrifuge in an Italian oil mill from olive oil fruits harvested in Apulia (Italy); the vertical centrifuge was applied on the above batch.

Approx. 6 L of each above batch were the VOO samples which were transferred to the laboratory both for characterization and for lab-scale centrifugation and sedimentation trials.

Chemicals: Diethyl ether, chloroform ($CHCl_3$), methanol (CH_3OH), acetone (C_3H_6O), and citric acid for the citrate buffer were of analytical grade (Carlo Erba Reagents, Milan, Italy). Deionized water was produced by the Milli-Q-system (Millipore SA, Molsheim, France).

Methods—Physicochemical and biological properties measurement of the VOO samples: The turbidity grade was measured in nephelometric turbidity units (NTU) using a Hach Model 2100AN turbidimeter (Hach, Loveland, CO, USA), which was previously calibrated with formazine standards (20–7500 NTU). The water content (% w/w) was measured using a 37858 Hydranal—Moisture Test Kit (Honeywell Fluka, Bucharest, Romania), and the water activity (A_w) was measured using a Rotronic Hygroskop DT hygrometer (Michell Italia Srl, Milan, Italy). The insoluble solid content was measured using the method described in Breschi et al.[8] The microbial contamination (log CFU g^{-1}) was measured according to the method by Zullo et al.[30] with the modifications described in Breschi et al.[8]

Protein and total amino acids contents measurement of the VOO samples: Proteins and amino acids were extracted from the precipitate which was obtained after washing VOO samples with diethyl ether and centrifugation. 10 mL of diethyl ether was added to 50 mL test tube containing 25 g of sample and the test tube was manually shaken for 1 min; then, the test tube was centrifuged (NEYA 8xs, Remi Elektrotechnik Ltd., Palghar, India) for 5 min at 4500 rpm (2828 G), and the supernatant was carefully removed. The above procedure was repeated three more times, adding every time 25 g of sample and 10 mL of diethyl ether. 10 mL of diethyl ether was also added to the precipitate in the test tube and the test tube, after manually shaking for 1 min, was centrifuged for 5 min at 4500 rpm; the supernatant was carefully removed. The above procedure was repeated three more times, adding every time 10 mL of diethyl ether. The precipitate was dried at room temperature for 20 min; 3 mL of distilled water was added to the precipitate, then the test tube was mixed by vortex for 1 min, kept in an ultrasonic bath for 15 min, and mixed again by vortex for 1 min.

Protein content in the above precipitate was measured using the Total Protein Kit—Micro Lowry, Peterson's Modification (Sigma-Aldrich, Darmstadt, Germany), following the kit instruction without protein precipitation; protein content (mg kg^{-1}) was quantified by a UV/VIS Lambda 10 spectrophotometer (Perkin Elmer, Waltham, USA) at 750 nm. Amino acids compounds in the precipitate were subjected to extraction and derivatization using the EZfaast Amino Acid Analysis Kit (Phenomenex, Torrance, USA) following the instruction given by the manufacturer. The used method was already described in Whittaker et al.[31] Briefly, 2 μL of derivatized amino acids solution was injected in 1:10 split mode into amino acid column at 300 °C in a Zebron ZB-AAA column (10 m × 0.25 mm × 0.25 μm). The used gas chromatograph (GC) was an Agilent 7890A (Agilent Technologies, Santa Clara, USA) equipped with an Agilent 5970 mass selective detector (Agilent Technologies, Santa Clara, USA). The GC oven was initially set to 110 °C, increasing the temperature up to 150 °C at 10 °C min^{-1}, and up to 320 °C at 20 °C min^{-1}. Quantification of amino acids was performed using the mixed amino acids standard solution provided by the above kit. The norvaline was used as internal standard.

Phospholipids content measurement of the VOO samples: Phospholipids were extracted from VOO samples using a Bligh & Dyer method, followed by purification with solid phase extraction (SPE) according to Lewe et al.[32] The identification of phospholipids was performed by gas chromatography using an Agilent 7890A (Agilent Technologies, Santa Clara, USA) equipped

with an HP-INNOWax column (50 m × 0.2 mm × 0.4 μm of internal film). Initial column temperature was held at 35 °C and 33 psi for 1 min, then increased to 180 °C at 30 °C min^{-1}, then to 260 °C at 3 °C min^{-1}, with a hold time of 3 min. The EI mass detector was operated at 230 °C and with an IE energy of 70 eV. The MassHunter Quantitative Analysis software (Agilent Technologies, Santa Clara, USA) was used for the quantitative and qualitative analysis.

Optical microscope and particles diameter measurement of the VOO samples: The VOO samples were analyzed during the lab-scale gravity sedimentation trials by optical microscopy using a Nikon Eclipse Ti–S Inverted Microscope. All micrographs were acquired using an objective with a 10X magnification at 20 ± 1 °C controlled by means of a heating stage with temperature control (PE94, LINKAM). All the optical micrographs were analyzed with an image processing software (ImageJ, v.1.49.p) to evaluate the mean dimension of cloudy appearance components. DLS method was performed on a Brookhaven instruments apparatus (BI 9000AT correlator and BI 200 SM goniometer) to measure the mean hydrodynamic diameter of cloudy appearance components during lab-scale gravity sedimentation. The light scattered from the sample was collected at 90° with respect to the incident light (Torus laser, LaserQuantum, UK, wavelength = 532 nm) and the scattered intensity was detected by a BI-APD detector. VOO samples after being homogenized by vortex were placed in glass tubes and immersed in a thermostated cell filled with decahydronaphthalene to match the glass refractive index. All measurements were collected at 25 °C. The field autocorrelation functions were analyzed through cumulant analysis[33] to extrapolate the mean diameter associated with the objects present in the VOO samples.

Lab-scale centrifugation trials of the VOO samples: Seven centrifuge tubes with 50 g of VOO sample were centrifuged (NEYA 8 xs, Remi Elektrotechnik Ltd., Palghar, India) at 4500 rpm (2828 G) for 0, 1, 3, 5, 7.5, 15, and 30 min. About 20 g of centrifuged sample was collected from the middle of the centrifuge tube and added in the vial for the turbidity grade measurement in NTU (see measurement method in Section *Physicochemical and biological properties measurement of the VOO samples*).

Lab-scale gravity sedimentation trials of the VOO samples: The *C#1*, *N*, *K*, and *M* samples (≈0.5 L) were stored in 1 L glass bottles in the dark at room temperature for the entire experiment. At different sedimentation times (0, 48, 65, 80, 209, 217, and 230 days), the bottles were manually mixed for 30 s prior to the sampling; an aliquot of sample (≈2 mL) was collected from the middle of the bottle and used for the measurement of mean hydrodynamic diameter by DLS. Optical micrographs were acquired on the above VOO samples (≈5 μL) at 65 and 217 days of sedimentation; optical micrographs were also acquired on the above VOO samples at 217 days of sedimentation without manually mixing.

Data Processing: Data of VOO properties and chemical composition were statistically processed according to a one-way analysis of variance using Statgraphics Centurion software (ver. XV, Statpoint Technologies, Warrenton, VA). The kinetic data were processed using Table Curve 2D Version 4 software (Systos Software Inc., Richmond, CA).

Acknowledgements

Conflict of Interest

The authors declare no conflict of interest.

Author Contributions

C.B. and G.F. contributed equally to this work. C.B.: Conceptualization; Investigation; Methodology; Writing—original draft. G.F.: Conceptualiza-

[1] G. Cinelli, M. Cofelice, F. Venditti, *Colloids Interfaces* **2020**, *4*, 38.
[2] J. A. Cayuela-Sanchez, B. Caballero-Guerrero, *Trends Food Sci. Technol.* **2019**, *83*, 78.
[3] B. A. Zullo, G. Ciafardini, *Eur. J. Lipid Sci. Technol.* **2018**, *120*, 1700309.
[4] C. Breschi, L. Guerrini, A. Parenti, P. Masella, L. Calamai, L. Lunetti, B. Zanoni, *Food Control* **2022**, *137*, 108931.
[5] G. Ciafardini, B. A. Zullo, *Food Microbiol.* **2018**, *70*, 245.
[6] D. Fiorini, M. C. Boarelli, P. Conti, B. Alfei, G. Caprioli, M. Ricciutelli, G. Sagratini, D. Fedeli, R. Gabbianelli, D. Pacetti, *Int. Food Res. J.* **2018**, *105*, 65.
[7] A. Koidis, E. Triantafillou, D. Boskou, *Eur. J. Lipid Sci. Technol.* **2008**, *110*, 164.
[8] C. Breschi, L. Guerrini, P. Domizio, G. Ferraro, L. Calamai, V. Canuti, P. Masella, A. Parenti, E. Fratini, G. Fia, B. Zanoni, *Eur. J. Lipid Sci. Technol.* **2019**, *121*, 1900195.
[9] J. Lozano-Sanchez, L. Cerretani, A. Bendini, A. Segura-Carretero, A. Fernandez-Gutierrez, *Trends Food Sci. Technol.* **2010**, *21*, 201.
[10] A. Koidis, D. Boskou, *Eur. J. Lipid Sci. Technol.* **2006**, *108*, 323.
[11] F. J. Hidalgo, M. Alaiz, R. Zamora, *Anal. Chem.* **2001**, *73*, 698.
[12] A. Xenakis, V. Papadimitriou, T. G. Sotiroudis, *Curr. Opin. Colloid Interface Sci.* **2010**, *15*, 55.
[13] A. Gila, A. Sanchez-Ortiz, G. Beltran, M. A. Bejaoui, M. P. Aguilera, A. Jimenez, *Eur. J. Lipid Sci. Technol.* **2020**, *122*, 1900426.
[14] K. B. Bubola, M. Lukic, I. Mofardin, A. Butumovic, O. Koprivnjak, *LWT–Food Sci. Technol.* **2017**, *84*, 370.
[15] G. Altieri, F. Genovese, A. Tauriello, G. C. Di Renzo, *J. Food Eng.* **2015**, *166*, 325.
[16] J. Lozano-Sanchez, L. Cerretani, A. Bendini, T. Gallina Toschi, A. Segura-Carretero, A. Fernadez-Gutierrez, *J. Agric. Food Chem.* **2012**, *60*, 3754.
[17] C. Breschi, L. Guerrini, F. Corti, L. Calamai, P. Domizio, A. Parenti, B. Zanoni, *Ital. J. Food Sci.* **2021**, *33*, 33.
[18] L. Guerrini, B. Zanoni, C. Breschi, G. Angeloni, P. Masella, L. Calamai, A. Parenti, *Molecules* **2020**, *25*, 420.
[19] M. Fortini, M. Migliorini, C. Cherubini, L. Cecchi, L. Calamai, *Talanta* **2017**, *165*, 641.
[20] G. Fregapane, V. Lavelli, S. León, J. Kapuralin, M. Desamparados Salvador, *Eur. J. Lipid Sci. Technol.* **2006**, *108*, 134.
[21] H. Jabeur, A. Zribi, M. Bouaziz, *Eur. J. Lipid Sci. Technol.* **2017**, *119*, 1500602.
[22] A. Bakhouche, J. Lozano-Sánchez, C. A. Ballus, M. Martínez-García, M. G. Velasco, A. O. Govantes, T. Gallina Toschi, A. Fernández-Gutiérrez, A. Segura-Carretero, *Food Control* **2014**, *40*, 292.
[23] L. Guerrini, C. Breschi, B. Zanoni, L. Calamai, G. Angeloni, P. Masella, A. Parenti, *Foods* **2020**, *9*, 1067.
[24] G. Veneziani, S. Esposto, A. Minnocci, A. Taticchi, S. Urbani, R. Selvaggini, B. Sordini, L. Sebastiani, M. Servili, *LWT–Food Sci. Technol.* **2018**, *94*, 87.
[25] E. Bakowska, A. Siger, M. Rudzinska, K. Dwiecki, *J. Sci. Food Agric.* **2022**, *102*, 488.
[26] E. S. Budilarto, A. Kamal-Eldin, *Eur. J. Lipid Sci. Technol.* **2015**, *117*, 1095.
[27] V. Papadimitriou, M. Dulle, W. Wachter, T. G. Sotiroudis, O. Glatter, A. Xenakis, *Food Biophys.* **2013**, *8*, 112.
[28] M. L. Clodoveo, R. H. Hbaieb, F. Kotti, G. Scarascia Mugnozza, M. Gargouri, *Compr. Rev. Food Sci. Food Saf.* **2014**, *13*, 135.
[29] D. J. McClements, in *Modern Biopolymer Science* (Eds: S. Kasapis, I. T. Norton, J. B. Ubbink), Academic Press, Elsevier, Amsterdam, The Netherlands **2009**, Ch. 4.
[30] B. A. Zullo, G. Cioccia, G. Ciafardini, *Food Microbiol.* **2010**, *27*, 1035.
[31] A. Whittaker, I. Marotti, G. Dinelli, L. Calamai, S. Romagnoli, M. Manzelli, E. Palchetti, V. Vecchio, S. Benedettelli, *J. Sci. Food Agric.* **2010**, *90*, 1968.
[32] N. Lewe, S. Hermans, G. Lear, L. T. Kelly, G. Thomson-Laing, B. Weisbrod, B. S. A. Wood, R. A. Keizers, J. R. Deslippe, *J. Microbiol. Methods* **2021**, *188*, 106271.
[33] B. J. Frisken, *Appl. Opt.* **2001**, *40*, 4087.